Second Stability in the ATF Torsatron

J. H. Harris, M. Murakami, B. A. Carreras, J. D. Bell, G. L. Bell,[a] T. S. Bigelow, L. A. Charlton, N. Dominguez, J. L. Dunlap, J. C. Glowienka, L. D. Horton, H. C. Howe, R. C. Isler, H. Kaneko,[b] R. R. Kindsfather,[c] J. N. Leboeuf, V. E. Lynch, M. M. Menon, R. N. Morris, G. H. Neilson, V. K. Paré, D. A. Rasmussen, J. B. Wilgen, and W. R. Wing

Oak Ridge National Laboratory, Oak Ridge, Tennessee 37831

(Received 3 May 1989)

Access to the MHD second stability regime has been achieved in the ATF torsatron. Experimental β values ($\beta_0 \leq 3\%$, with fast ions contributing $\approx \frac{1}{3}$ of the pressure at high β) are well above the theoretical transition value ($\beta_c \approx 1.3\%$ for ideal modes) required to reach this regime. The relatively low β_c results from operation with peaked pressure profiles. The measured magnetic fluctuations decrease with increasing β, and the pressure profile broadens. This behavior is consistent with theoretical predictions for β self-stabilization of resistive interchange modes.

PACS numbers: 52.55.Hc, 52.30.Jb, 52.35.Py

The ideal magnetohydrodynamic (MHD) second stability regime has attracted increasing attention in toroidal confinement fusion research[1,2] because it offers the hope of operation at high $\beta \equiv 2\mu_0 p/B^2$ (the ratio of the plasma kinetic pressure to the magnetic pressure) with favorable confinement, which would improve the prospects for a viable D-T fusion reactor. This theory predicts that the changes in the internal magnetic surfaces (plasma axis shift and shape) caused by an increase in plasma pressure act to stabilize instabilities driven by unfavorable field-line curvature.[1] As a result, the plasma can become more stable as β increases ("β self-stabilization"), with an accompanying reduction in the anomalous transport induced by the curvature-driven instabilities. In this Letter we describe experiments in which operation in the second stability regime has been achieved at relatively low β in a torsatron (a type of stellarator).

Because of their external control of magnetic configuration and the absence of plasma current, stellarators are well suited for exploring the second stability regime and studying β self-stabilization. In stellarators with significant shear ($d\chi/dr > 0$, where χ is the rotational transform and r is the plasma minor radius) the dominant instabilities are interchange modes.[3,4] These modes can be stabilized by the magnetic well produced by the outward magnetic axis shift at finite β (Shafranov shift), and this β self-stabilization effect can open a stable path to the second stability regime.[5,6] The ATF torsatron design was optimized to explore this possibility.[7]

ATF is an $l = 2$, twelve-field-period torsatron with major radius $R_0 = 2.10$ m, average minor radius $\bar{a} = 0.27$ m, magnetic field on axis $B_0 < 2$ T, central rotational transform $\chi_0 \approx 0.3$, and edge transform $\chi_a \approx 1$. For the profile assumed in the ATF design studies[6] the β self-stabilization effect should dominate at $\beta_0 \approx 5\%$. Electron-beam field mapping in early 1988 revealed substantial magnetic islands (6 cm wide at the $\chi = \frac{1}{2}$ surface and smaller at other rational surfaces).[8] These islands, now corrected, acted as a magnetic limiter and effectively reduced the plasma radius to $r_p \approx 0.6\bar{a}$ (increasing the effective aspect ratio A from 8 to 10) and the effective edge transform $\chi_a \approx 0.5$. This led to a large increase in the Shafranov shift ($\delta/a \propto \beta_0 A/\chi_a^2$) that enhanced the self-stabilization effect and afforded the results reported here, which show β self-stabilization of MHD activity.

In this Letter we first discuss the experimental conditions and describe measurements of magnetic fluctuations; we then compare these results with theoretical stability predictions.

Figure 1(a) shows some of the characteristics of a typical discharge.[9] Up to 1.4 MW of H^0 power is injected from co- and/or counter-oriented neutral beams into a H^+ target plasma produced with second-harmonic electron-cyclotron heating (ECH) using a 0.2-MW, 53-GHz gyrotron at $B_0 = 0.95$ T. The plasma current ranges from near zero for balanced neutral-beam injection (NBI) to a maximum of 4.2 kA for unidirectional NBI, but the general characteristics of the discharge do

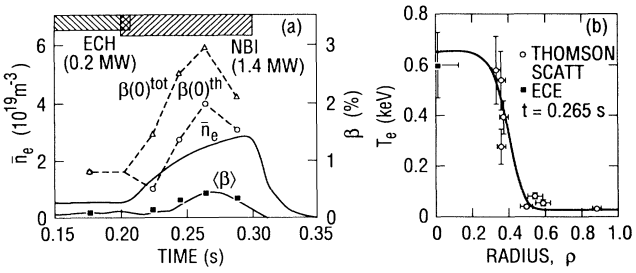

FIG. 1. (a) Time history of an ATF discharge. The upper and lower β_0 curves show the total (including fast-ion contribution) and thermal pressures, respectively. For the $\langle\beta\rangle$ curve, the smooth trace represents the diamagnetic measurement, and the solid points come from the profile analysis. (b) Electron temperature profile.

not depend strongly on beam configuration. The volume-average β, measured with a diamagnetic loop and defined using the full plasma radius $\bar{a}=0.27$ m, reached $\langle\beta\rangle=0.5\%$ at a line-average electron density $\bar{n}_e \approx 2.5\times10^{19}$ m^{-3}, central density $n_{e0}\approx 5\times10^{19}$ m^{-3}, central electron temperature [measured by Thomson scattering and third-harmonic electron-cyclotron emission (ECE)] $T_{e0}\approx 0.6$ keV, and ion temperature (from impurity ion spectroscopy) $T_{i0}\approx 0.26$ keV at the time of the maximum $\langle\beta\rangle$, $t=0.265$ s in Fig. 1(a). For this case, the central β is $\beta_0\approx 3\%$ [Fig. 1(a)], and the global-energy confinement time $\tau_E^*\approx 5$ ms. Figure 1(a) shows both total and thermal plasma β_0, as determined from analysis of the measured profiles and from beam deposition and heating calculations.[9] Typically, about one-third of the plasma pressure at high β comes from the fast ions produced by NBI. Figure 1(b) shows the T_e profile reconstructed from measurements along a vertical chord at $R_0=2.10$ m. The data are plotted in flux coordinates (based on the three-dimensional finite-β equilibrium[10]), for which ρ is the mean plasma radius normalized to $\bar{a}$. Similarly narrow T_e profiles were observed in both ECH and NBI phases and are believed to be caused by the islands at $\chi\geq\frac{1}{2}$. The outward Shafranov shift is large for relatively low values of β: $\delta=0.11$ m$\approx 2r_p/3$ for $\beta_0=3\%$. Such a large shift lowers the ultimate equilibrium β limit to $\beta_0\approx 5\%$ (which is still above the values achieved in the experiment) but also lowers the β_c at which self-stabilization becomes dominant.

Although the field errors constrict the plasma pressure profile $p(\rho)$, we do see evidence of changes in $p(\rho)$ as β increases. We define a parameter $\langle\beta\rangle/\bar{n}_e T_{e0}$ as a convenient measure of the "broadness" of the profile. Here T_{e0} is determined from ECE measurements. Figure 2(a) shows this parameter (and the corresponding $\langle\beta\rangle/\beta_0$ based on several profile-analyzed cases) as a function of $\langle\beta\rangle$ for the discharges analyzed in the fluctuation studies described below. The pressure profiles broaden substantially as $\langle\beta\rangle$ increases to $\sim 0.2\%$. The time histories of the broadness for individual discharges show a similar dependence on β suggesting that the trend in Fig. 2(a) is not merely the result of differing beam configurations. This behavior does not correlate as well with the variations of radiative cooling and NBI power deposition.

The fluctuation measurements[11] on ATF were made with a soft-x-ray detector array viewing the central portion of the plasma ($\rho\leq 0.5$) and, for poloidal magnetic fluctuations ($\tilde{B}_\theta$), Mirnov coils located ≈ 30 cm outside the plasma. Three coil pairs were separated only in toroidal angle ($\Delta\phi=30°$, 150°, and 180°), and one pair was separated only in poloidal angle ($\Delta\theta=150°$). The soft-x-ray signals show no evidence of instabilities. Spectral correlation analysis of the $\tilde{B}_\theta$ signals reveals bands of high-coherence fluctuations (frequency-resolved coherent function $\gamma>0.7$, where $\gamma=1$ indicates perfect coherence, even at the largest coil separations) in the frequency range 5–60 kHz with amplitudes $\sim 10^{-3}$ G. The relative phase shifts of the signals from the toroidally displaced coils indicate predominantly $n=1$ toroidal mode symmetry with some evidence of higher-n structure. Assignment of poloidal mode numbers (m) to the $n=1$ fluctuations is complicated by the noncircular flux surface shape and strong Shafranov shift. The data can be interpreted most simply in terms of two principal components, $m=2$ in the frequency range 5–20 kHz and $m=3$ in the range 20–45 kHz.

Figure 3 shows the rms coherent $n=1$ components of $\tilde{B}_\theta$ in the frequency range 5–60 kHz (determined during ECH and at peak β during NBI) plotted as a function of $\langle\beta\rangle$ for a sequence of discharges. The amplitude-limit curve of the data suggests that $\langle\tilde{B}(n=1)\rangle$ rises with β

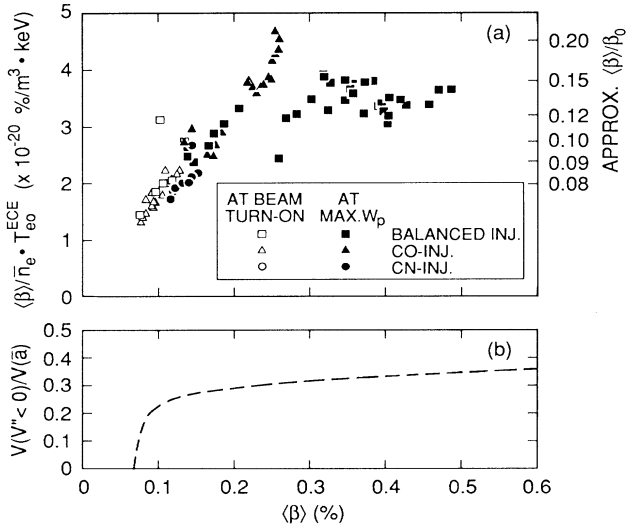

FIG. 2. (a) Profile broadening parameter $\langle\beta\rangle/\bar{n}_e T_{e0}$ vs $\langle\beta\rangle$ for the discharges shown in Fig. 3, and (b) calculated volume of the region of the plasma with $V''<0$ (magnetic well).

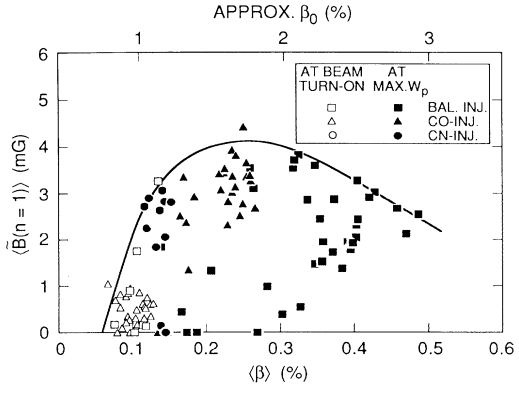

FIG. 3. Dependence of rms (in the frequency band 5–60 kHz) coherent $n=1$ poloidal magnetic fluctuation amplitude, $\langle\tilde{B}(n=1)\rangle$, on $\langle\beta\rangle$.

for $\langle\beta\rangle \leq 0.2\%$, but then saturates and begins to decrease as $\langle\beta\rangle$ exceeds 0.3%. Of course, the trajectory of a given discharge in the $\langle\tilde{B}\rangle$ vs $\langle\beta\rangle$ space of Fig. 3 depends on the evolution of profiles, etc., and we infer that this is the cause of the scatter in the data. The time histories of $\langle\tilde{B}\rangle$ in individual discharges (e.g., Fig. 4) appear to recapitulate the curve in Fig. 3; $\langle\tilde{B}\rangle$ rises proportionally with $\langle\beta\rangle$ for $\langle\beta\rangle < 0.3\%$ and then decreases as $\langle\beta\rangle$ exceeds this value. During the thermal collapse phase,[9] $\langle\tilde{B}\rangle$ again varies proportionally with $\langle\beta\rangle$ when $\langle\beta\rangle < 0.3\%$.

The behavior of $\langle\tilde{B}\rangle$ with increasing $\langle\beta\rangle$ cannot be attributed simply to the finite-β plasma shift, since the Mirnov coils used to measure $\langle\tilde{B}\rangle$ in Figs. 3 and 4 are located on the large-major-radius side of the torus: At finite β, the plasma actually moves closer to these coils. The time variations of the principal components of $\tilde{B}$ show that the decrease of $\langle\tilde{B}(n=1)\rangle$ for $\langle\beta\rangle > 0.3\%$ (Figs. 3 and 4) is most strongly reflected in the 5–20-kHz component (assigned $m=2$), while the 20–45-kHz ($m=3$) component changes little.

Since there is no Ohmic current in ATF, we can quantify the fast-ion density n_f by measuring the beam-driven current for varying unidirectional injection power and find (experimentally) that $n_f \propto P_b/\bar{n}_e^{1.5}$. For the high-$\beta$ experiments, $P_b/\bar{n}_e^{1.5}$ varies by a factor of 2–3, and trend analysis shows no correlation between this quantity and $\langle\tilde{B}\rangle$. Furthermore, during individual discharges [Fig. 1(a)], the fast-ion pressure remains nearly constant while the fluctuations vary with total $\langle\beta\rangle$. These results suggest that the fluctuations in ATF are not driven by tangential injection *per se*.[12] Additional studies show no obvious correlation of $\langle\tilde{B}\rangle$ with beam configuration or plasma current.

Theoretical ideal MHD stability studies[13] were carried out for two sequences of equilibria. In the first, $p(\rho)$ was fixed to have the peaked shape measured in the experiment at high β [Fig. 1(b)] for the entire range of $\langle\beta\rangle$. In the second sequence, $p(\rho)$ was allowed to evolve from an even narrower profile at low β to the high-β profile along the path indicated for the experiment [Fig. 2(a)]. These equilibria are all stable to low-n ($n \leq 3$) modes. However, the Mercier criterion[14] ($D_M > 0$ for stability) gives indications of instability for the fixed-profile sequence. It therefore describes the overall plasma stability properties. The sign of the shear term is opposite that in tokamaks so that ballooning modes are not important.[3] Figure 5(a) shows the Mercier unstable region and the contours for relevant low-order resonances as a function of $\langle\beta\rangle$ mean radius for the fixed-profile equilibrium sequence. At a given radius (e.g., $\rho=0.52$, where D_M has its maximum negative value), D_M shows weak instability for $0.25\% < \beta_0 < 1.1\%$ (corresponding to $0.05\% < \langle\beta\rangle < 0.25\%$). The transition to second stability for the whole radial range occurs at relatively low β_0 ($=1.3\%$, corresponding to $\langle\beta\rangle=0.3\%$). Above this value, D_M increases sharply, reflecting a strong β self-stabilization effect. The experimental values (β_0 up to 3%) are well above the theoretical transition value. For the second equilibrium sequence, in which $p(\rho)$ broadens with increasing β, the Mercier unstable region disappears altogether, suggesting that the plasma remains close to marginal stability along the path to second stability.

Even in the second stability regime the plasma remains unstable to dissipative modes, particularly resistive interchange modes. However, β self-stabilization is expected to reduce the saturation amplitude of these modes as β increases.[15] In Fig. 5(b), $\tilde{B}$ at saturation for a single-helicity calculation ($n/m=2/5$) is plotted versus $\langle\beta\rangle$ for the fixed-profile equilibrium sequence. The fluctuation amplitude increases strongly when $\langle\beta\rangle$ is in the Mercier unstable region, but decreases at $\langle\beta\rangle > 0.2\%$ ow-

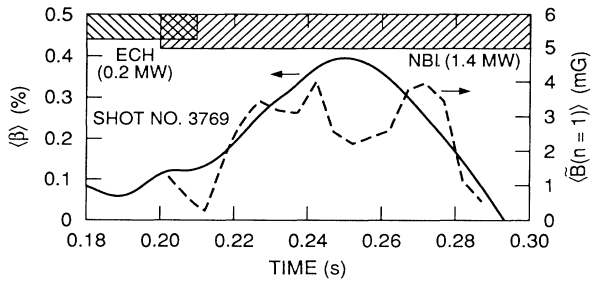

FIG. 4. Time dependence of $\langle\tilde{B}(n=1)\rangle$ and $\langle\beta\rangle$ for a sample discharge with balanced neutral injection.

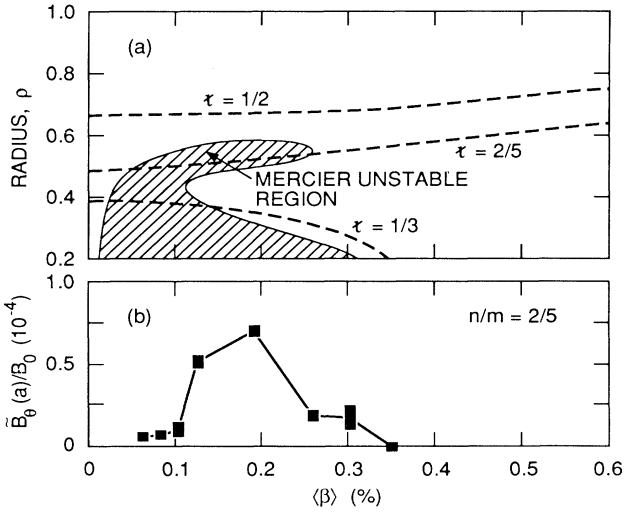

FIG. 5. (a) Ideal Mercier instability diagram for ATF with peaked pressure profile. The dashed lines show the trajectories of the principal resonant surfaces. (b) Theoretical poloidal magnetic fluctuation amplitudes at saturation at the plasma edge for single-helicity ($n/m=2/5$) resistive pressure-gradient-driven modes as a function of $\langle\beta\rangle$ for the fixed-profile equilibrium sequence.

ing to β self-stabilization. For multiple-helicity calculations including the toroidal mode couplings, the $\tilde{B}_\theta$ spectrum at the plasma edge is dominated by the lowest n modes ($n=1$, $m=2$ and $n=1$, $m=3$).[13] These features are similar to those observed in the experiment, but the experimental values of $\tilde{B}$ are smaller (by a factor ≥ 10) than those shown in Fig. 5(b), which may imply that ω^* and other kinetic effects should be included in the modeling.

The β self-stabilization results from the radial expansion of the region with magnetic well ($V'' < 0$), coupled with an increase in the magnitude of the favorable V''. The calculated $\langle\beta\rangle$ dependence of the volume of the magnetic well is shown in Fig. 2(b). The dependence is similar to that of the pressure-profile broadening observed in the experiment. This similarity could be evidence of improved plasma confinement due to stabilization, but measurements connecting local transport and fluctuations and clearly delineating the effects of beam configuration are needed to substantiate this interpretation. Such studies are planned for ATF.

We acknowledge with appreciation the contributions of our many colleagues in the ATF group. This research was sponsored by the Office of Fusion Energy, U.S. Department of Energy, under Contract No. DE-AC05-84OR21400 with Martin Marietta Energy Systems, Inc. One of the authors (H.K.) participated in these experiments as part of a U.S.-Japan exchange in fusion research.

---

[a]Permanent address: Auburn University, Auburn, AL 36849.

[b]Permanent address: Plasma Physics Laboratory, Kyoto University, Kyoto, Japan.

[c]Present address: Igen, Inc., 1530 East Jefferson Street, Rockville, MD 20852.

[1]A. M. Mikhailovskii and V. D. Shafranov, Zh. Eksp. Teor. Fiz. **66**, 190 (1974) [Sov. Phys. JETP **39**, 88 (1974)]; B. Coppi, A. Ferriera, J. W.-K. Mark, and J. J. Ramos, Nucl. Fusion **19**, 715 (1979); L. M. Kovrizhnykh and S. V. Shchepetov, Fiz. Plazmy **6**, 976 (1980) [Sov. J. Plasma Phys. **6**, 533 (1980)].

[2]G. A. Navratil *et al.*, in *Proceedings of the Eleventh International Conference on Plasma Physics and Controlled Nuclear Fusion Research, Kyoto, 1986* (IAEA, Vienna, 1987), Vol. 1, p. 299; T. C. Simonen *et al.*, in *Proceedings of the Twelfth International Conference on Plasma Physics and Controlled Nuclear Fusion Research, Nice, 1988* (IAEA, Vienna, 1989) [IAEA Report No. IAEA-CN-50/E-3-6 (to be published)]; S. C. Luckhardt *et al.*, Phys. Rev. Lett. **62**, 1508 (1989); M. Okabayashi *et al.*, in *Proceedings of the Eleventh International Conference on Plasma Physics and Controlled Nuclear Fusion Research, Kyoto, 1986* (IAEA, Vienna, 1987), Vol. 1, p. 275.

[3]V. D. Shafranov, Phys. Fluids **26**, 357 (1983).

[4]N. R. Ainsworth *et al.*, in *Proceedings of the Seventh International Conference on Plasma Physics and Controlled Nuclear Fusion Research, Innsbruck, 1978* (IAEA, Vienna, 1979), Vol. 1, p. 745; J. H. Harris *et al.*, Phys. Rev. Lett. **53**, 2242 (1984).

[5]L. M. Kovrizhnykh and S. V. Shchepetov, Fiz. Plazmy **7**, 419 (1981) [Sov. J. Plasma Phys. **7**, 229 (1981)].

[6]B. A. Carreras *et al.*, Phys. Fluids **26**, 3569 (1983).

[7]J. F. Lyon *et al.*, Fusion Technol. **10**, 179 (1986).

[8]R. J. Colchin *et al.*, in *Proceedings of the Sixteenth European Conference on Controlled Fusion and Plasma Physics, Venice, 1989* (European Physical Society, Petit-Lancy, Switzerland, 1989), Vol. 13B, Pt. 2, p. 615.

[9]M. Murakami *et al.*, in Ref. 8, Vol. 13B, Pt. 2, p. 595.

[10]S. P. Hirshman, W. I. van Rij, and P. Merkel, Comput. Phys. Commun. **43**, 143 (1986).

[11]J. H. Harris *et al.* (to be published).

[12]W. W. Heidbrink *et al.*, Phys. Rev. Lett. **57**, 835 (1986).

[13]B. A. Carreras *et al.*, Oak Ridge National Laboratory Report No. ORNL/TM-11102, 1989 (unpublished).

[14]C. Mercier, Nucl. Fusion **1**, 47 (1960); N. Dominguez *et al.*, Oak Ridge National Laboratory Report No. ORNL/P-89/1086, 1989 (unpublished).

[15]B. A. Carreras, Comments Plasma Phys. Controlled Fusion **12**, 35 (1988).